



## Approximate Delaunay mesh reconstruction and quality estimation from point samples



Wenyong Gong<sup>a</sup>, Yong-Jin Liu<sup>b,\*</sup>, Kai Tang<sup>c</sup>, Tieru Wu<sup>a</sup>

<sup>a</sup> Institute of Mathematics, Jilin University, Changchun, 130012, China

<sup>b</sup> TNList, Department of Computer Science and Technology, Tsinghua University, Beijing, 100084, China

<sup>c</sup> Department of Mechanical and Aerospace Engineering, Hong Kong University of Science and Technology, Hong Kong, China

### HIGHLIGHTS

- We present proof for mesh reconstruction from points that gives the upper and lower bounds of mesh quality.
- A practical approximate Delaunay mesh reconstruction method is proposed.
- Experiments show that our method works well on real-world point cloud.

### ARTICLE INFO

#### Article history:

Received 4 March 2012

Received in revised form 25 March 2014

#### Keywords:

Surface sampling

Mesh quality

Delaunay triangulation

2-manifold mesh reconstruction

### ABSTRACT

Several sampling criteria had been proposed for  $C^2$  smooth surfaces such that the reconstructed meshes from point samples are homeomorphic to the original surfaces. In this paper, based on a widely used sample criterion, we present proofs that give the upper and lower bounds of mesh quality (in terms of several triangle aspect ratios) for the reconstructed mesh. To make the proposed theoretical bounds useful in practical applications with real-world point data, we propose a novel mesh reconstruction method that works in three steps: (1) approximate Delaunay mesh reconstruction; (2) point data upsampling and (3) hole filling. Finally, examples are presented, which illustrate the effectiveness of the proposed method.

© 2014 Elsevier B.V. All rights reserved.

## 1. Introduction

Surface sampling criteria had been widely studied in various fields of science and engineering. On one hand, surface sampling is a fundamental problem, and mathematicians study it with interest of representing a surface using a homomorphic mesh reconstructed from dense points [1]. On the other hand, computer scientists and engineers are also interested, since they approximate natural or man-made objects satisfying necessary constraints (positional and normal field convergence, see below) in addition to the topology [2]. Furthermore, surface sampling criteria have direct influence on the quality of reconstructed meshes.

Mesh reconstruction from point samples is often required to possess several properties: (1) homeomorphism to the original surfaces; (2) positional convergence, which ensures that the Hausdorff distance between the mesh and the original surface is small when the point samples are dense enough; (3) normal field convergence, which ensures that the normal fields between the mesh and the original surface are close to each other. Dai et al. [2] point out that positional convergence

\* Corresponding author.

E-mail addresses: [liuyongjin@tsinghua.edu.cn](mailto:liuyongjin@tsinghua.edu.cn), [liu.yongjin@gmail.com](mailto:liu.yongjin@gmail.com) (Y.-J. Liu).

does not guarantee the normal field convergence. Currently many methods such as [3,4] just consider the first property. In this paper, we present surface sampling criteria in a combinatorial manner which considers all the above three properties for the mesh reconstruction.

Many sampling and reconstruction methods are based on the Voronoi/Delaunay paradigm [3,5,6,1,7]. These methods have rigorous theoretical guarantee for output, but their computation have to resort to some quantities in  $R^3$  such as the local feature size (i.e., the distance from points on the surface to the medial axis). There are mainly two types of Voronoi diagrams involved in representing and reconstructing a surface using point samples: restricted Voronoi diagram (rVd) [8,9] and intrinsic Voronoi diagram (iVd) [10]. Let  $P$  be a set of sample points on a surface  $S$  in  $R^3$ . For each  $p \in P$ , the Voronoi cell  $V(p)$  of  $p$  can be defined as

$$V(p) = \{x \in R^3 : \|p - x\| \leq \|q - x\|, \forall q \in P\}. \quad (1)$$

The Voronoi diagram of  $P$  is the boundaries of Voronoi cells of all the points in  $P$ . A restricted Voronoi cell is the intersection of the Voronoi cell  $V(p)$  with  $S$ . Edelsbrunner and Shah [9] proved that if rVd satisfies the closed ball property (see Section 3), the rDt (dual of rVd) is homeomorphic to  $S$ . If we replace the embedded space  $R^3$  in Eq. (1) by  $S$ , we obtain the definition of the intrinsic Voronoi diagram, in which the Euclidean metric  $\|\cdot\|$  changes to the geodesic metric  $\|\cdot\|_S$  [11]. Recently Liu et al. [12] proved that the complexity of geodesic Voronoi diagrams is closely related to point numbers and face numbers. Algorithmic computation of iVd on 2-manifold has been proposed in [13,6]. If the sampling  $P$  is sufficiently dense such that between any two samples there is a unique geodesic (more details are presented in Section 2), iVd has as dual the *intrinsic Delaunay triangulation* (iDt). iVd satisfying the closed ball property also guarantees a homeomorphic manifold iDt. The method studied in this paper is based on an intrinsic Voronoi sampling.

Most previous work on surface sampling and mesh reconstruction can be classified into two classes: (1) theoretic part about sampling criteria, but cannot be implemented directly [4,1]; (2) practical algorithms, but lack of support with theoretical background [14]. For the former, Leiben et al. [1] presented one of the earliest work in the Delaunay triangulation of general Riemannian manifolds. Their main contribution is the proof of the existence of the Delaunay triangulation under a rigorous sampling criterion. Since this sampling criterion is related to the local feature size, it is too strict to be feasible in most practical algorithms. The work in [2] gives some analytical estimations to ensure the positional and normal consistency, and a sampling criterion is also presented. Based on the convexity radius and injectivity radius, a loose sampling criterion (see Eq. (2) in Section 3) is proposed by Dyer et al. [4], but it can only guarantee the homeomorphism without any guaranty of positional or normal convergence. Motivated by these works, in this paper we present theoretical bounds of a mesh quality measure based on a sampling criterion in [2]. In this paper we propose a practical approximate iDt mesh reconstruction algorithm with theoretical guarantee. The algorithm can output high quality meshes when point samples satisfy our sampling criteria. The output of our algorithm are exact Delaunay triangulations in the planar case. For points sampled from a 2-manifold surface, our algorithm outputs a good approximation of the Delaunay triangulation.

For practical surface reconstruction algorithms,  $\alpha$ -shape [15] can be used to reconstruct surfaces from a dense unstructured set of points. The shortcoming of this algorithm is that a reasonable  $\alpha$  need to be chosen manually. The *Crust* proposed by Amenta et al. [3] is the first Delaunay triangulation algorithm with a theoretically topological guarantee for a well sampled point set. Several variants for *Crust* [5,16,17] are developed later, and all these algorithms ensure the homeomorphism between the reconstructed  $M$  and the original surface  $S$ . *Cocone* in [18] is a fast surface reconstruction algorithm which also guarantees homeomorphism. Subsequently robust *Cocone* [19] and super *Cocone* [20] are presented to handle noisy and large point clouds, respectively. Liu and Yuen [21] also use a quadratic optimization technique to reconstruct unstructured points. These methods all use the ambient Euclidean space and can be regarded as extrinsic methods.

For a point set in the Euclidean plane, the Delaunay triangulation maximizes the minimum angle in all possible triangulations. In this sense, the Delaunay triangulation generally constructs a high quality mesh. Although the quality of a mesh has been estimated by using many methods [22,23], that for a iDt mesh on 2-manifolds has never been considered. Inspired by the image super-resolution technique [24], we present a new upsampling method which can add enough points until the point set satisfies our sampling requirement. In this paper, we (1) give a theoretical bound to the estimation of the iDt mesh quality using the proposed sampling criterion, and (2) generate this bound into practical methods for handling real-world point data, including mesh reconstruction, point data upsampling and hole filling. The main contributions of this paper include:

- The theoretical bounds of a mesh quality measure based on the sampling criterion are established.
- An incremental algorithm using an edge propagation scheme to reconstruct the approximate iDt mesh from point samples is proposed.
- An upsampling scheme is proposed, which can convert a real-world point cloud into a point set satisfying the proposed sampling criterion. Moreover, a details-preserving hole filling method is also proposed to repair incomplete point data.

The rest of this paper is organized as follows. In Section 2, some preliminaries are reviewed, and our main results are also presented. An incremental algorithm which reconstructs the approximate iDt mesh from a point cloud is presented in Section 3. Some examples are shown in Section 4. Finally, the paper is concluded in Section 5.

## 2. Mesh quality estimation

In this section, we give some necessary concepts in the Riemannian geometry [25–27], followed by a mesh quality estimation.

### 2.1. Preliminaries

We assume that  $S$  is a compact, smooth and connected 2-manifold surface without boundary embedded in  $R^3$ . The geodesic distance is the length of the shortest geodesic between two points on a 2-manifold. An embedded curve  $\gamma$  on  $S$  parameterized by arc-length is a geodesic if  $\gamma''$  is normal to  $S$  at every point of  $\gamma$ .

We denote  $T_pS$  the tangent plane of  $S$  at  $p$ . Let  $v \in T_pS$  be a tangent vector at  $p \in S$ . The exponential map of  $p$  is a mapping  $exp_p : T_pS \rightarrow S$  which is defined by  $exp_p(v) = \gamma_v(1)$ , where  $\gamma_v : [0, 1] \rightarrow S$  is the unique geodesic in  $S$  with  $\gamma_v(0) = p$ ,  $\gamma_v(1) = v$ . If  $p \in S$ , let  $B(p, r) = \{x \in S : d_s(p, x) < r\}$  and  $B_{T_pS}(0, r) = \{x \in T_pS : d(p, x) < r\}$ , where  $r > 0$ ,  $d_s(\cdot, \cdot)$  and  $d(\cdot, \cdot)$  represent the geodesic and Euclidean distance respectively.

The main difficulty of the Delaunay triangulation on 2-manifolds is the non-uniqueness of geodesics joining two points on  $S$ . The *injectivity radius* is introduced to characterize the unique geodesic between two points. The injectivity radius at a point  $p \in S$ , denoted  $inj(p)$ , is the supremum of the radii  $r$  for which the exponential map  $exp_p : B_{T_pS}(0, r) \rightarrow B(p, r)$  is injective. The injectivity radius of  $S$ , denoted  $inj(S)$ , is the infimum of the injectivity radii at all points on  $S$ . In fact there is a unique geodesic joining two points if their geodesic distance is not greater than one of the injectivity radii of both points.

An open set  $S'$  of  $S$  is called strongly convex if any two points  $p, q \in S'$  can be joined by exactly one geodesic which is entirely contained by  $S'$ . Strongly convex sets are a useful tool for investigating local properties of surfaces, and moreover *convexity radius* tells us how large it is. For any  $x \in S$ , the convexity radius  $conv(x)$  of  $x$  is defined by  $conv(x) = \sup\{\rho : B(x, r) \text{ is convex for all } r < \rho\}$ . The strong convexity radius  $conv(S)$  of  $S$  is the infimum of the radii at all points on  $S$ .

### 2.2. Mesh quality estimation

Dyer et al. [4] give an intrinsic sampling criterion similar to ours as proposed below. But geometric accuracy and mesh quality are not analyzed in [4]. In this section, we establish the theoretic bounds for the iDt mesh quality.

**Definition 1** (*Intrinsic Voronoi Diagram*). For a given point set  $P = \{p_1, p_2, \dots, p_n\} \subset S$ , the Voronoi cell  $V(p_i)$  of  $p_i$  is defined as

$$V(p_i) = \{x \in S : d_s(x, p_i) \leq d_s(x, q), \forall q \in P\}.$$

The intrinsic Voronoi diagram (iVd for short)  $V(P)$  is the union of all the Voronoi cells of  $P$ , and it is also a covering of  $S$ .

Hereafter  $P$  represents a sample point set in  $S$ .

The iVd is well-defined [4] if it satisfies the closed ball property [9]:

- Each Voronoi cell is a closed topological disk;
- The intersection of two Voronoi cells is either empty or a single Voronoi edge;
- The intersection of three Voronoi cells is either empty or a single Voronoi vertex.

The iDt of  $P$  is a triangulation of  $S$  by connecting samples lying in neighboring Voronoi cells with geodesics. An iDt is well-defined if its duality (the corresponding iVd) is well-defined. The iDt mesh is constructed by using line segments to replace the geodesic in iDt.

The topological consistence is an elementary requirement for surface reconstruction. We adopt the sampling condition [4] to ensure the homeomorphism between the surface and its iDt mesh. For some  $\varepsilon$ , if  $\forall x \in S, \exists p_i \in P$  such that  $p_i \in B(x, \varepsilon)$ , we say that the point set  $P$  satisfies the  $\varepsilon$ -sampling condition, where  $\varepsilon$  is called the sampling radius. For every  $x \in S$ , if

$$\rho_m(x) = \min \left\{ conv(x), \frac{1}{2} inj(x) \right\} \tag{2}$$

then the iDt of  $P$  in  $S$  is well-defined if  $P$  is a  $\rho_m$ -sampling of  $S$  [4]. Moreover the iDt mesh of  $P$  is homeomorphic to  $S$ .

Good appearances of real-world objects also need to consider the positional and normal convergence in addition to the homeomorphism. We use the following result in [2].

**Theorem 1** ([2]). *Let  $M$  be an iDt mesh of  $P$ . Suppose the principal curvature upper bound of  $S$  is  $\kappa$ , and  $P$  satisfies the  $\varepsilon$ -sampling for  $\varepsilon \leq \frac{1}{8\kappa}$ . Then the Hausdorff distance  $d_H(M, S) \leq 4\kappa\varepsilon^2$ , and the normal distance  $d_n(M, S) \leq 9\kappa\varepsilon$ , where  $d_H(M, S) = \inf\{\delta > 0 : M \subset U_\delta(S), S \subset U_\delta(M)\}$  with  $U_\delta(M) = \{x \in R^3 : \exists y \in M. t. d(x, y) < \delta\}$ , and  $d_n(M, S) = \max_{s \in S} |n(s) - n(s')|$  with  $n(s)$  the unit normal vector at  $s$  and  $s' \in M$  the nearest point of  $s$ .*

Given these previous results on topological convergence, positional convergence and normal convergence, we next use them to analyze the mesh quality.

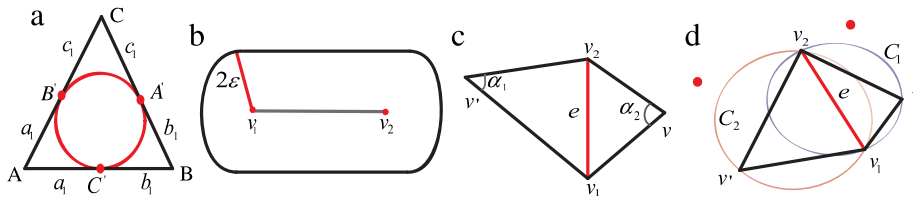


**Fig. 1.** (a) The triangle  $\triangle ABC$  and its three tangent points. (b) The capsule of a front edge. (c) A quadrilateral formed by two neighboring triangles. (d) New added triangle is empty for  $cap(e)$ .

**Theorem 2.** Assuming that  $P$  is a  $\varepsilon$ -sampling of  $S$ , and let  $\widetilde{\triangle ABC}$  be any Delaunay triangle in  $S$ , the principal curvature bound is  $\kappa > 0$ , and its minimal edge length is  $\tilde{l} \geq \frac{1}{2}\varepsilon$ .  $T_{ABC}$  is the planar triangle corresponding to  $\widetilde{\triangle ABC}$ . Assume  $l$  and  $R$  are the shortest edge length and the circumradius of  $T_{ABC}$  respectively, then  $\frac{1}{2} - \frac{\kappa^2 \varepsilon^2}{48} \leq \frac{l}{R} \leq \sqrt{3}$ .

**Proof.** Assume that  $AB$  is the edge with the shortest length in  $T_{ABC}$ ,  $\widetilde{AB}$  is the shortest geodesic in  $S$  joining  $A$  and  $B$  with length  $\tilde{l}$ . Let  $R(t)$  be the arc length parameterization of  $\widetilde{AB}$ ,  $0 \leq t \leq \tilde{l}$ ,  $\vec{m} = \frac{R(\tilde{l}) - R(0)}{|R(\tilde{l}) - R(0)|}$ . According to the proof of Lemma 1 in [2], we have  $l = |AB| = |R(\tilde{l}) - R(0)| \geq |R(\tilde{l}) - R(0)| \cdot (R'(t), \vec{m}) \geq \tilde{l} - \frac{\kappa^2 \tilde{l}^3}{6}$ . Let function  $f(\tilde{l}) = \tilde{l} - \frac{\kappa^2 \tilde{l}^3}{6}$ , then  $f'(\tilde{l}) = 1 - \frac{1}{2}\kappa^2 \tilde{l}^2$ .  $f(\tilde{l})$  is an increasing function if  $\kappa \tilde{l} \leq \sqrt{2}$ . Thus the inequality  $l \geq \frac{1}{2}\varepsilon - \frac{\kappa^2 \varepsilon^3}{48}$  holds. Suppose the circumcircle of  $\widetilde{\triangle ABC}$  is  $D$ , then there is no interior point belonging to  $P$ . We assert the radius of  $D$  is no greater than  $\varepsilon$ , since otherwise we can find a geodesic disk inside  $D$  of radius  $\varepsilon$ , then  $D$  at least contains a point of  $P$  different from  $A, B, C$  as its interior. Thus  $R \leq \varepsilon$ . Now we have the conclusion  $\frac{l}{R} \geq \frac{1}{2} - \frac{\kappa^2 \varepsilon^2}{48}$ . On the other hand, we also have  $R = \frac{l}{2\sin(\alpha)}$  according to elementary geometry, where  $\alpha$  is the opposite angle about the minimal edge  $l$ . Since  $\alpha \leq 60^\circ$ , then  $\frac{l}{R} \leq \sqrt{3}$ .

**Lemma 1.** For a given planar triangle  $\triangle ABC$ , let  $r$  and  $L$  be the inradius and maximal edge length, then  $\frac{r}{L} \leq \frac{\sqrt{3}}{6}$ .

**Proof.** Assuming  $a, b, c$  are the edge length and  $R$  is the circumradius of  $\triangle ABC$ ,  $A', B', C'$  are three tangent points of  $\triangle ABC$  and its incircle. We also assume that  $a = b_1 + c_1, b = a_1 + c_1, c = a_1 + b_1$  (see Fig. 1(a)). Firstly two elementary geometry relationships are given without proof. If the area of  $\triangle ABC$  is  $s$ , then  $R = \frac{abc}{4s}$  and  $r = \frac{2s}{a+b+c}$ . Let  $p = a_1 + b_1 + c_1, a_1 = px, b_1 = py, c_1 = pz$  and note  $x + y + z = 1$ , then  $s = \sqrt{pa_1b_1c_1}, r = \sqrt{\frac{a_1b_1c_1}{a_1+b_1+c_1}} = p\sqrt{\frac{xyz}{x+y+z}}, R = \frac{(a_1+c_1)(b_1+c_1)(a_1+b_1)}{4\sqrt{pa_1b_1c_1}} = \frac{p}{4} \frac{(x+y)(y+z)(x+z)}{\sqrt{xyz}}$ . Then  $\frac{1}{r} + \frac{1}{R} = \frac{1}{p\sqrt{xyz}} + \frac{4\sqrt{xyz}}{p(x+y)(y+z)(x+z)} \cdot \frac{1}{a} + \frac{1}{b} + \frac{1}{c} = \frac{1}{p} (\frac{1}{x+y} + \frac{1}{y+z} + \frac{1}{x+z})$ . We note that  $x^2y^2 + y^2z^2 + x^2z^2 - xyz = x^2y^2 + y^2z^2 + x^2z^2 - xyz(x+y+z) = \frac{1}{2}((xy-yz)^2 + (xz-yz)^2 + (xy-xz)^2) \geq 0$ , i.e.  $xyz \leq x^2y^2 + y^2z^2 + x^2z^2$ , thus we can derive  $\sqrt{3xyz} \leq xy + yz + xz$ . According to the arithmetic-geometric inequality,  $\frac{1}{3} = \frac{x+y+z}{3} \geq \sqrt[3]{xyz}$ , thus  $\sqrt{3xyz} \leq 1$ . Let  $E = \sqrt{3xyz}((y+z)(x+z) + (x+y)(x+z) + (x+y)(y+z)) - (x+y)(y+z)(x+z) - 4xyz = \sqrt{3xyz}(1 + xy + yz + xz) - xy - xz - yz - 3xyz = (\sqrt{3xyz} - 1)(xy + yz + xz - \sqrt{3xyz}) \leq 0$ , then  $\sqrt{3}(\frac{1}{a} + \frac{1}{b} + \frac{1}{c}) - \frac{1}{r} - \frac{1}{R} = \frac{E}{p\sqrt{xyz}(x+y)(y+z)(x+z)} \leq 0$ , i.e.  $\sqrt{3}(\frac{1}{a} + \frac{1}{b} + \frac{1}{c}) \leq \frac{1}{r} + \frac{1}{R}$ . According to Euler's inequality  $R \geq 2r$ , then the conclusion  $\frac{r}{L} \leq \frac{\sqrt{3}}{6}$  holds.

**Theorem 3.** Assuming that  $P$  is a  $\varepsilon$ -sampling of  $S$ , let  $\widetilde{\triangle ABC}$  be a Delaunay triangle in  $S$ , the principal curvature bound is  $\kappa > 0$  and its minimal edge length is  $\tilde{l} \geq \frac{\varepsilon}{2}$ .  $T_{ABC}$  is the planar triangle corresponding to  $\widetilde{\triangle ABC}$ . Assume  $L$  and  $r$  are the maximal edge length and inradius of  $T_{ABC}$  respectively, and  $P$  satisfies the  $\varepsilon$ -sampling of  $S$ . Then  $\frac{1}{48}(1 - \frac{1}{24}\kappa^2\varepsilon^2)^2 \leq \frac{r}{L} \leq \frac{\sqrt{3}}{6}$ .

**Proof.** Assuming that  $s, a, b, c$  are the area and edge length of  $\triangle ABC$ , and we also let  $l, R$  be the minimal edge length and circumradius. Since  $R = \frac{abc}{4s}, r = \frac{2s}{a+b+c}$  according to the elementary geometry, thus  $r = \frac{abc}{2R(a+b+c)} \geq \frac{l^3}{6LR}$ . In light of the proof of last theorem  $l \geq \frac{\varepsilon}{2} - \frac{\kappa^2 \varepsilon^3}{48}, R \leq \varepsilon$ , then we have  $\frac{r}{L} \geq \frac{1}{48}(1 - \frac{1}{24}\kappa^2\varepsilon^2)^2$ . On the other hand,  $\frac{r}{L} \leq \frac{\sqrt{3}}{6}$ . We thus accomplish the conclusion.

According to the theorems above, we have the following corollary.

**Corollary 1.** Suppose that the principal curvature upper bound of  $S$  is  $\kappa$ . Let  $\varepsilon \leq \min\{conv(S), \frac{1}{2}inj(S), \frac{1}{8\kappa}\}$ ,  $P$  satisfies  $\varepsilon$ -sampling. Then the  $iDt$  mesh of  $P$  is homeomorphic to  $S$ ; the Hausdorff distance  $d_H(M, S) \leq 4\kappa\varepsilon^2$ ; the normal distance  $d_n(M, S) \leq 9\kappa\varepsilon$ ; the ratio between the shortest edge length  $l$  and the circumradius  $R$  of a triangle  $\frac{1}{2} - \frac{\kappa^2 \varepsilon^2}{48} \leq \frac{l}{R} \leq \sqrt{3}$ ; the ratio between the inradius  $r$  and the maximal edge length  $L$  of a triangle  $\frac{1}{48}(1 - \frac{1}{24}\kappa^2\varepsilon^2)^2 \leq \frac{r}{L} \leq \frac{\sqrt{3}}{6}$ .

**Table 1**  
Pseudocode of approximate iDt mesh reconstruction algorithm.

Approximate iDt mesh reconstruction algorithm
1. Find a seed triangle $T_s = \{e_1, e_2, e_3\}$ .
2. Initialization: $E = \{e_1, e_2, e_3\}, T = \{T_s\}$ .
3. while (for each edge $e$ in $E$ ).
4. If $e$ is a common edge of two triangles, do nothing.
5. Choose a point $v$ from $cap(e)$ . Assuming the starting and ending points of $e$ are $v_1$ and $v_2$ respectively, construct a new triangle $t = \{v_1, v, v_2\}$ , and add $t$ into $T$ .
6. $flip(e)$ and push the two new edges into the edge queue.
7. end while.

### 3. Mesh reconstruction from real-world point data

Point samples which satisfy the criterion used in Section 3 is usually required to be very dense and real-world point data seldom satisfy it. Real-world point data also frequently have holes (e.g., due to the occlusion of concave regions).

In this section, we propose a three-step mesh reconstruction method which can guarantee a good mesh quality.

#### 3.1. Approximate Delaunay mesh reconstruction

Mesh reconstruction from points is fairly ubiquitous in various fields [28,29,17,30]. Motivated by the ball-pivoting algorithm [14], we propose an edge propagation scheme and present a new incremental reconstruction algorithm to approximate the iDt mesh of a point set  $P$ . If an edge  $e = \{v_1, v_2\}$  in a mesh under construction appears in just one triangle, it is called a front edge. A front edge may be a boundary edge. A capsule of an edge  $e = \{v_1, v_2\}$  is a point set in which the distance from every point to  $e$  is no greater than  $2\varepsilon$  (see Fig. 1(b)). We define  $cap(e)$  to be the subset of  $P$  which is contained by the capsule of  $e$ . Therefore,  $cap(e)$  represents the candidate points to be chosen. Note that  $cap(e)$  is not empty according to our sampling requirement.

Let  $T$  be the approximate iDt mesh of  $P$  and  $E$  the queue of an edge front. The basic mesh reconstruction algorithm is shown in Table 1 and some key parts are explained below. Seeking a proper seed triangle is of importance for reconstruction. The seed triangle should satisfy that its minimal circumscribing ball contains no points of  $P$ , thus the triangle is Delaunay. Note that the edge  $e$  in step 4 with opposite orientations is regarded as the same one.

When constructing a new triangle using the current front edge  $e$ , a new point  $v$  is selected from  $cap(e)$  in step 5. The point  $v$  satisfies: (1) the angle  $\alpha_2$  (see Fig. 1(c)) at  $v$  is the largest among all points in  $cap(e)$ ; (2) the newly added triangle does not create a non-manifold. If  $\alpha_1 + \alpha_2 > \pi$ , the  $flip(e)$  operation which is equal to the classical edge flipping method is performed. Given a proper edge length threshold, our reconstruction algorithm can also construct surfaces with boundaries.

In addition, our reconstruction method has the following property. A triangle is empty if its circumcircle contains no points of  $P$  in the planar case. If the chosen point  $v$  has the largest angle among all the points in  $cap(e)$ , then in the planar case the circumcircle of the newly added triangle is empty for  $cap(e)$  if the circumcircle of the triangle sharing edge  $e$  is also empty. We now give a brief proof about the above statement. Assume that the newly added triangle is  $\Delta v_1 v v_2$  and its neighboring triangle is  $\Delta v' v_1 v_2$ . Their corresponding circumcircles are  $C_1$  and  $C_2$ , respectively. See Fig. 1(d) for an illustration. If there exists a point  $\tilde{v}$  which is inside  $C_1$ , then the angle  $\angle v_1 \tilde{v} v_2$  is larger than  $\angle v_1 v v_2$ . This contradicts the assumption that the angle at  $v$  is the largest. If a planar point set is given, our proposed algorithm strictly outputs the Delaunay triangulation. While when the sample points distributed in a 2-manifold space, our algorithm is only an approximation. Since the point samples are usually very dense to satisfy the sampling criteria, locally points are sampled sufficiently in the tangent plane around each sample points, and thus our approximation algorithm performs well in practical cases as demonstrated by our experiments. In  $R^3$ , this statement clearly holds if we consider the minimal circumsphere of a triangle. It is worth noting that in the planar case the chosen point  $v$  is in front of  $e$  since otherwise a non-manifold would be created.

#### 3.2. Point data upsampling

The initial approximate Delaunay mesh outputs an optimal mesh which interpolates the original point data. However, due to the deficiencies inherent in the original data (e.g., undersampling and holes), the initial mesh may be often not as good as we have expected. In the step 2 of our method, we propose an upsampling scheme based on the initial mesh. Then in the next step (Section 3.3), we deal with holes inside the mesh.

For a given point cloud  $P$ , it may have places which do not satisfy our sampling criterion, therefore an upsampling procedure is required. In this subsection we present a novel upsampling method which is used to output a point data satisfying our sampling criterion. Our method is based on the following assumption: the overall surface usually has consistent point patterns or shape textures and small patches around points on the surface are frequently similar to each other.

If the sampling criterion is not satisfied at a point  $p \in P$ , we construct a new point and use its signature to find a similar patch for upsampling  $P$  locally around  $p$  to guarantee the sampling criterion. Let  $N = \{p_1, p_2, \dots, p_k\}$  be the  $k$ -nearest neighbors of  $p$ , and  $p_1$  the nearest point of  $p$ , then we seek a point  $p_k$  from  $N - \{p_1\}$  such that the triangle  $\Delta p p_1 p_k$  made of  $p$ ,

$p_1$  and  $p_k$  has the minimal maximum angle. Let  $p'$  be the circumcenter of  $\triangle pp_1p_k$ , then we make use of the two dimensional Gaussian kernel function centered on  $p'$  as weights to construct a new point  $p_{new}$ .

$$z(p_{new}) = \frac{\sum_{r \in N' \cup p'} z(r) \cdot w(r, p')}{\sum_{r \in N' \cup p'} w(r, p')},$$

where  $w(r, p') = e^{-d(r-p')^2/h^2}$ , and the window width  $h$  here is set to the sampling radius  $\varepsilon$ . In addition, XY coordinates can be calculated in the same way.

After constructing an initial new point  $p_{new}$ , we next seek a most similar point  $\tilde{p}$  from  $P$  to refine  $p_{new}$  with the aid of geometry signature. Suppose the  $k$ -nearest neighbors of  $p_{new}$  is  $q_j$  ( $j = 1, 2, \dots, k$ ), and further assume that  $H_j$  and  $G_j$  are the mean curvature and Gaussian curvature at  $q_j$ , respectively. Then the geometry signature of the point patch  $\Omega = \{q_j\}_{j=1}^{k+1}$  ( $q_{k+1} = p_{new}$ ) consists of eight ingredients  $f_1, f_2, f_3, f_4, f_5, f_6, f_7, f_8$ :

$$\begin{aligned} f_1 &= \min\{H_j\}, & f_2 &= \max\{H_j\}, & f_3 &= \min\{G_j\}, & f_4 &= \max\{G_j\}, \\ f_5 &= \frac{f_2}{f_1}, & f_6 &= \frac{f_4}{f_3}, & f_7 &= \sum_j H_j / (k + 1), & f_8 &= \sum_j G_j / (k + 1). \end{aligned}$$

Note that the mean curvature and Gaussian curvature at every point are estimated by fitting a local quadric surface here.

For the surface patch  $\Omega$ , we need to compare it with other surface patches to seek a maximum similarity surface patch. Let  $f_{i,1}, f_{i,2}, f_{i,3}, f_{i,4}, f_{i,5}, f_{i,6}$  be the geometry signatures of another surface patch  $\Omega_i$ , we define the following function  $S(\Omega, \Omega_i)$  ( $S_i$  for short) to measure their similarity:

$$S(\Omega, \Omega_i) = \sum_j \frac{(f_j - f_{i,j})^2}{f_j + f_{i,j} - f_j f_{i,j}}.$$

The greater the value of  $S(\Omega, \Omega_i)$  is, the more similar the two surface patches  $\Omega$  and  $\Omega_i$  are.

According to the value of  $S(\Omega, \Omega_i)$ , we could seek a most similar surface patch  $\Omega^*$  as a candidate to refine the point  $p_{new}$ . To complete this task, both patches  $\Omega$  and  $\Omega^*$  should be aligned by using a rigid transformation. In this work, we utilize the iterative closest point (ICP) algorithm to accomplish the registration between the two patches. Let  $T$  be the  $4 \times 4$  rigid transformation matrix. Let  $\omega_j \in \Omega^*$  be the nearest point of  $q_j \in \Omega$ , and the distance between  $\Omega$  and  $\Omega^*$  is given by

$$d(\Omega, \Omega^*) = \sum_j \|q_j - \omega_j\|^2.$$

Then the optimal rigid transformation matrix  $T^*$  is determined by the following optimization problem:

$$T^* = \text{argMin}_T d(\Omega, T(\Omega^*)),$$

where  $T(\Omega^*)$  means every point in  $\Omega^*$  is transformed by  $T$ .

Finally the refined point  $\tilde{p} \in T^*(\Omega^*)$  is the nearest point of  $p_{new}$ , which is also the point to be added into  $P$ .

### 3.3. Detail-preserving hole filling

In real-world situations, holes may exist in the point data. Before processing such a point cloud, we first need to complete it. A general hole-filling process consists of two steps: detect all holes of a point cloud, and then fill the holes. Since many algorithms [31] have been known for hole detections, we mainly focus on how to fill the holes such that the filled regions satisfy our sampling criterion.

Our hole-filling procedure also comprises two steps. Assuming that  $H$  is the boundary (point set) of a hole, we initially cover the hole  $H$  by using the advancing front method. The initial point cloud patch, however, is often not satisfactory, and thus we propose a method to refine these points. Next, we describe the two steps in details.

Let  $H = \{v_1, v_2, \dots, v_k\}$  be the boundary points of a hole, an improvement for the advancing front algorithm [32] is given as follows.

1. Initialize front  $F = \{v_1, v_2, \dots, v_k\}$ .
2. Calculate the angle  $\theta_j$  for each point  $v_j$  about its adjacent boundary edges.
3. For the point  $v_i$  with the smallest angle  $\theta_i$ , create new points and triangles according to three rules in Fig. 2.
4. Update the point front  $F$ .
5. Repeat (2) through (4) until the whole hole is covered by points.

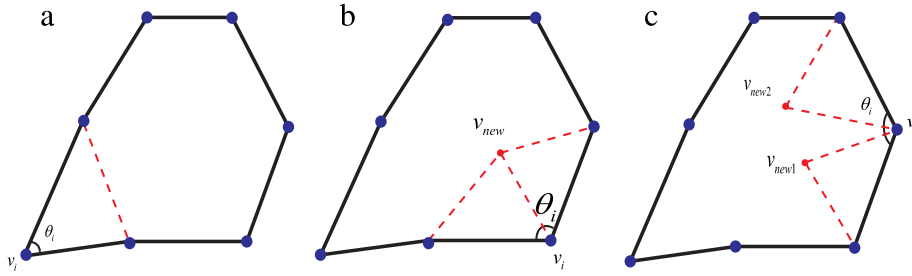


Fig. 2. Create initial points using three rules, and the black edges are the hole boundaries. (a)  $\theta_i \leq 75^\circ$ . (b)  $75^\circ < \theta_i \leq 135^\circ$ . (c)  $\theta_i > 135^\circ$ .

If  $\theta_i \leq 75^\circ$ , two neighboring points are connected (see Fig. 2(a)), note that the front is not necessary to update in this case. When  $75^\circ < \theta_i \leq 135^\circ$  (see Fig. 2(b)), one new point  $v_{new}$  lies in the bisector of  $\theta_i$ , and the distance from  $v_{new}$  to  $v_i$  is the average of lengths of adjacent boundary edges of  $v_i$ . If  $\theta_i > 135^\circ$ , two new equilateral triangles are created, and two new points are inserted into  $F$  (see Fig. 2(c)).

After obtaining an initial point cloud patch to cover  $H$ , we next describe how to use the Poisson equation to optimize these new points.

Assuming that  $g$  is an ideal guidance vector field of  $H$ , and  $f$  is a scalar function defined on all the points of  $H$ . Then we want to minimize the following variational function:

$$\min_f \int \|\nabla f - g\|^2, \quad \text{with } f|_{\partial H} = f^*|_{\partial H},$$

where  $f^*$  is a known scalar function defined on  $\partial H$ , and  $\nabla = (\frac{\partial}{\partial x}, \frac{\partial}{\partial y}, \frac{\partial}{\partial z})$  is the gradient operator. In fact, the minimization problem is equivalent to the Poisson equation with the Dirichlet boundary condition.

$$\Delta f = \text{div}g, \quad \text{with } f|_{\partial H} = f^*|_{\partial H},$$

where  $\Delta f = \frac{\partial^2 f}{\partial x^2} + \frac{\partial^2 f}{\partial y^2} + \frac{\partial^2 f}{\partial z^2}$  is the Laplacian operator, and  $\text{div}g$  is the divergence of  $g$ . Furthermore, if  $g$  is the gradient of some guidance function  $\phi$ , solving the Poisson equation is equivalent to solving the Laplacian equation.

$$\Delta \tilde{f} = 0, \quad \text{with } \tilde{f}|_{\partial H} = f^*|_{\partial H} - \phi|_{\partial H}. \tag{3}$$

Therefore the final outcome is simply  $f = \tilde{f} + \phi$ . Obviously  $\tilde{f}$  is a harmonic function which interpolates  $f^* - \phi$ .

However, if we solve the Laplacian equation directly, the result may be unsatisfactory. Therefore the newly added points  $\{v_j^{new}\}$  are rotated  $\frac{\pi}{2}$  counterclockwise with respect to their corresponding axes, respectively, and then these points are optimized by solving the Laplacian equation.

First, we introduce how to calculate the normals which are used to determine the rotation axes. The discrete Laplacian–Beltrami operator [33] on a point cloud  $P = \{P_1, P_2, \dots, P_n\}$  is defined as an  $n \times n$  matrix as follows:

$$L[i][j] = \begin{cases} G(i, j) & i \neq j \\ G(i, i) - \sum_{j=1}^n G(i, j) & \text{otherwise} \end{cases} \tag{4}$$

where  $G(i, j) = -\frac{1}{(4\pi h)^{3/2}} \cdot \frac{A_j}{4} \cdot e^{-\|P_i - P_j\|^2 / 4h}$ , and  $h$  is the kernel support size, and  $A_j$  is the area of all triangles incident to  $P_j$ . More details can be found in [33].

By prescribing the Dirichlet boundary condition, at least two boundary points (e.g.  $u_i = 1, u_j = -1$ ) are needed, we could construct a harmonic function  $\mathbf{u}$  using the following equation:

$$L\mathbf{u} = \mathbf{0}.$$

Note that  $L$  is a symmetric and positive semi-definite matrix, and therefore the equation can be solved by many methods such as the conjugate gradient (CG).

Furthermore, we also could take advantage of this equation to estimate the normals of points as soon as the boundary conditions are given. For the new points  $\{v_j^{new}\}$ , for example, if  $\mathbf{u}$  is the normal coordinate, we can easily obtain normals' coordinates when the normals of boundary points are given. Note that  $x$ -,  $y$ - and  $z$ - coordinates need to be calculated three times. Then the rotation axis of each point  $v_j^{new}$  is the one passing through the barycenter of the  $k$ -nearest neighbors of  $v_j^{new}$  with orientation  $n_j$ , where  $n_j$  is the normal of  $v_j^{new}$ .

Now we describe how to obtain the Laplacian solver of Eq. (3). In fact, with a small variation, the discrete Laplacian–Beltrami stated above can approximate the Laplacian operator  $\nabla^2$  and be used to solve this equation:

$$\tilde{L}[i][j] = \begin{cases} G(i, j) & i \neq j \\ G(i, i) - \sum_{j \in N(i)} G(i, j) & \text{otherwise,} \end{cases}$$

where  $N(i)$  is the  $k$ -nearest neighbors of  $v_i^{new}$ , and  $G(i, j)$  is the same as that in (4).

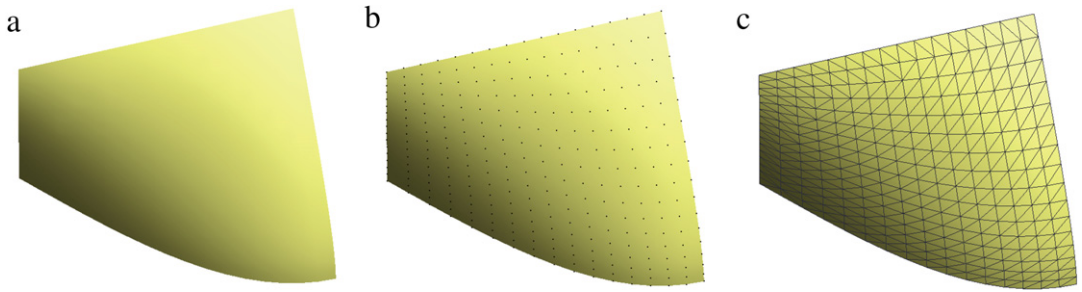


**Fig. 3.** (a) Parametric surface  $r(u, v) = (u, v, \cos(u)\sin(v))$ ,  $u, v \in [0, \frac{\pi}{2}]$ . (b) Sample point set satisfying our sampling requirement. (c) Approximate iDt mesh.

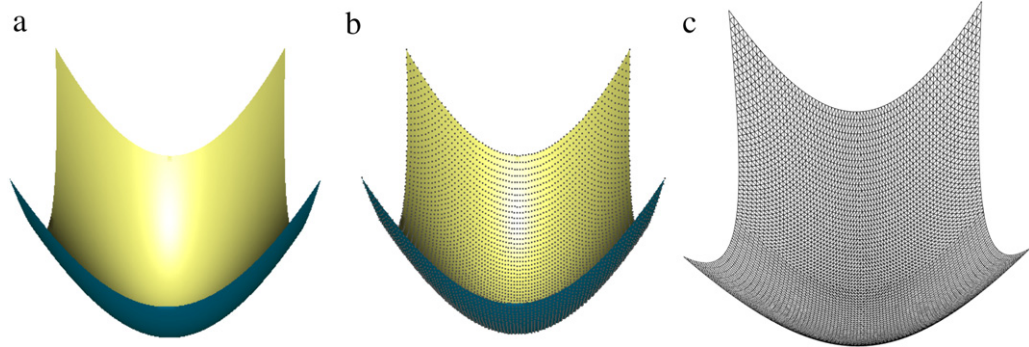


**Fig. 4.** (a) Implicit surface  $z = x^2 + y^2$ ,  $x, y \in [-1, 1]$ . (b) Sample point set satisfying our sampling requirement. (c) Approximate iDt mesh.

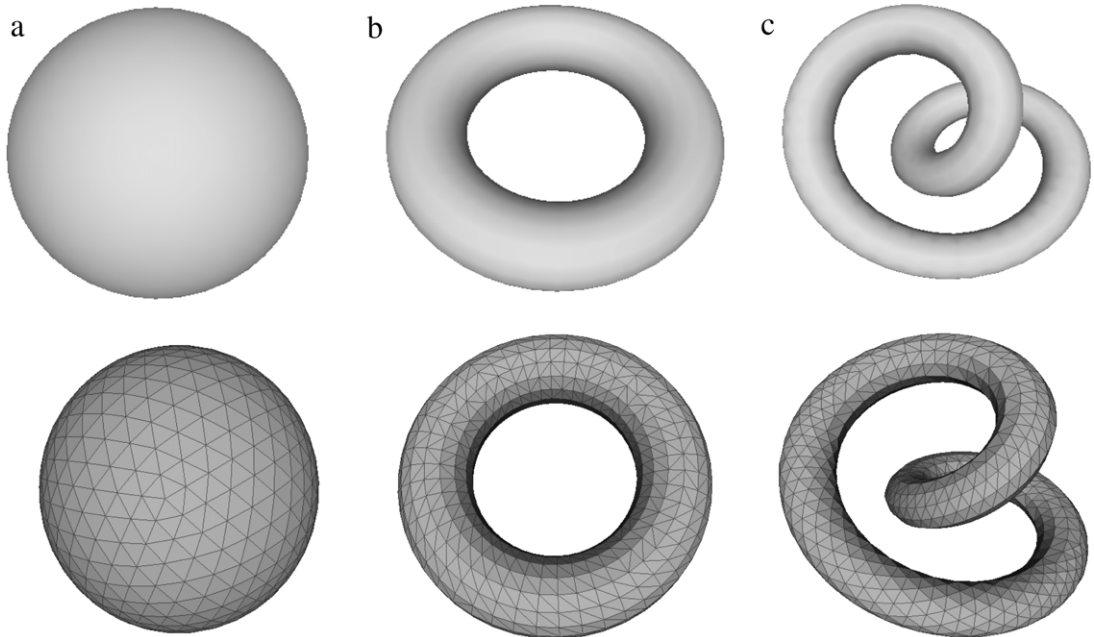


**Fig. 5.** Smooth surfaces are approximated by triangular meshes. (a) Unit sphere and its reconstruction mesh. (b) Torus and its reconstruction mesh. (c) Knot and its reconstruction mesh.

By applying the discrete Laplacian–Beltrami operator  $\tilde{L}$  to Eq. (3) with the boundary condition, the equation can be formulated as a sparse linear system

$$\tilde{A}\mathbf{f} = \mathbf{b}.$$

This linear system can be solved by the conjugate gradient method.

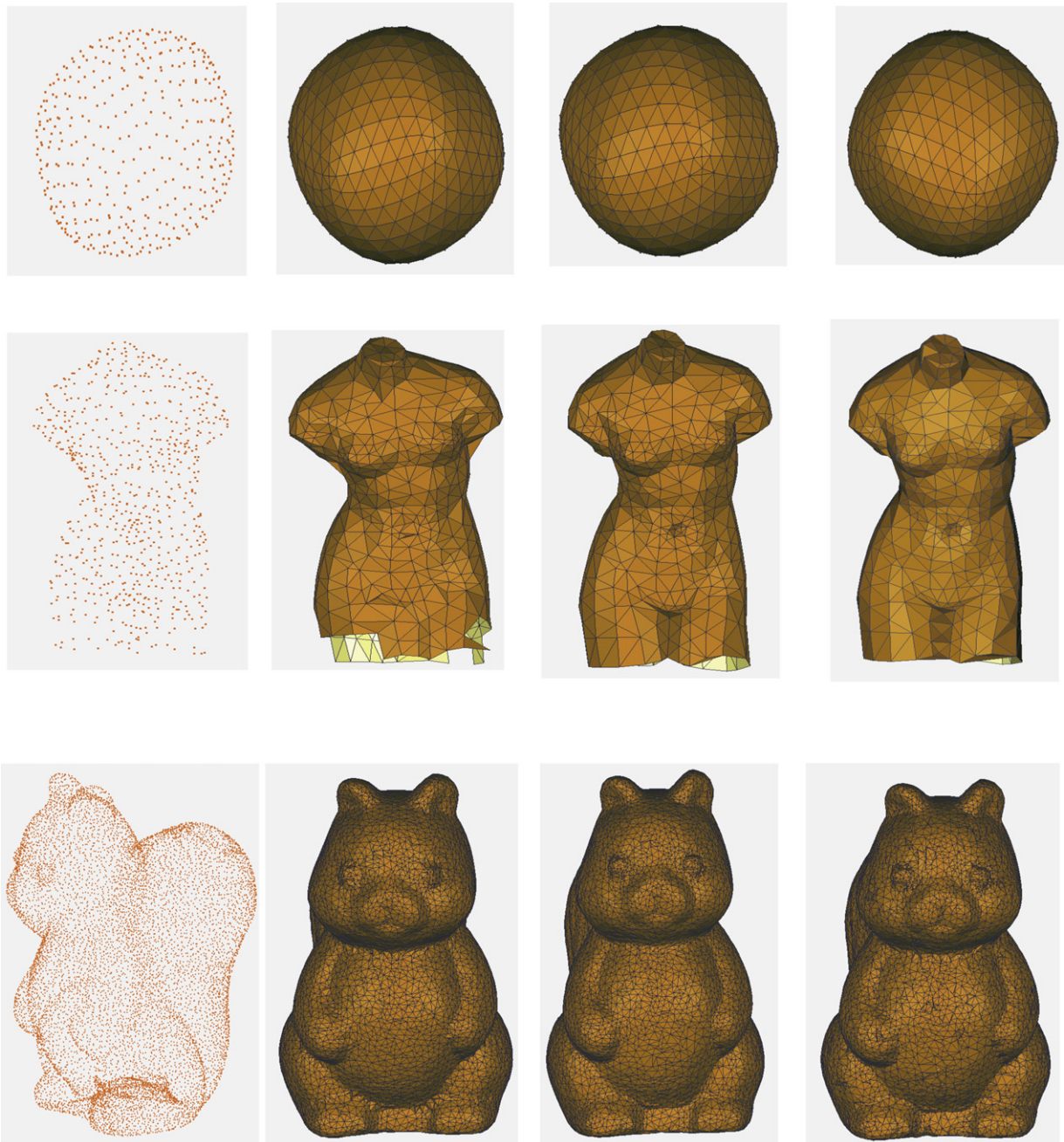


**Fig. 6.** Point sets are shown in the first column. Reconstructions shown in the second, third and fourth columns are generated by the ball-pivoting algorithm [14], *Crust* algorithm [5] and our algorithm, respectively.

#### 4. Experimental results

To test and verify our algorithms on practical examples, the sampling on a parametric surface is performed, and the comparison between the theoretical and practical quality estimations is performed next. Given a densely sampled point cloud, we reconstruct the approximate iDt mesh using our algorithm. For the hole region of a point cloud, we perform the hole filling algorithm. The following examples show the effectiveness of our method.

We take the parametric surface  $r(u, v) = (u, v, \cos(u)\sin(v))$ ,  $u, v \in [0, \frac{\pi}{2}]$  (see Fig. 3(a)) to test our sampling requirement. For the  $u$  (or  $v$ ) curve segment  $s(u)$  (or  $s(v)$ ) on  $r(u, v)$ , assuming the parametric domain to be  $[0, l] \times [0, l]$ , we have  $s(u) \leq \sqrt{2}l$ ,  $s(v) \leq \sqrt{2}l$ . Thus the resampling on  $r(u, v)$  can be accomplished in the parametric domain. When taking  $\varepsilon = 0.1$  the sampling criterion is satisfied. Thus in the parametric domain we draw a  $16 \times 16$  grid (boundaries are contained), and

**Table 2**

The practical calculation results of mesh quality for several 2-manifolds in Fig. 5.

Model	#vertices	#faces	$(\frac{l}{R})_0$	$(\frac{l}{R})_\infty$	$(\frac{r}{L})_0$	$(\frac{r}{L})_\infty$
Sphere	642	1280	1.62	1.732	0.255	0.289
Torus	768	1536	1.14	1.444	0.194	0.215
Knot	1262	2524	0.819	1.727	0.126	0.235

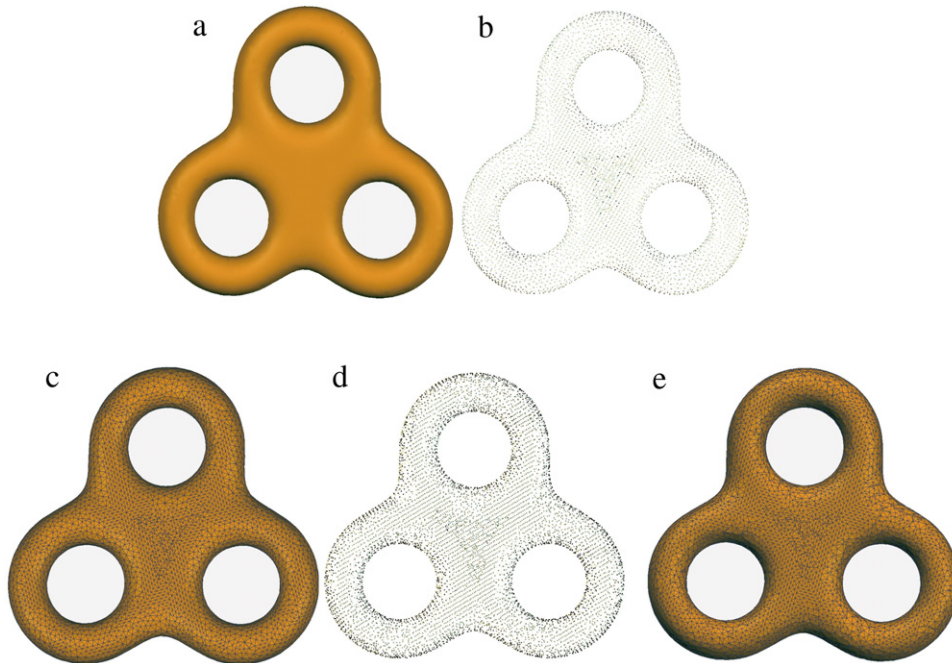


**Fig. 7.** (a) Tri-torus surface. (b) Initial point data. (c) Reconstruction surface of (b). (d) Upsampling point data of (b). (e) Reconstruction surface of (d).

points on  $r(u, v)$  mapping from crossing points are what we need. See Fig. 3(b) for an illustration. The ultimate reconstructed mesh is also shown in Fig. 3(c). Fig. 4 shows a sampling on the implicit surface  $z = x^2 + y^2$ ,  $x, y \in [-1, 1]$ .

For several smooth 2-manifolds (see Fig. 5) that have parametric representations, we can directly calculate their principle curvatures. For the sampling radius  $\varepsilon = \frac{1}{8\kappa}$ , where  $\kappa$  is the upper bound of principal curvatures, the ratio between the shortest edge length  $l$  and the circumradius  $R$  is  $0.5 \leq \frac{l}{R} \leq 1.732$ , and the ratio between the incircle radius  $r$  and the maximal edge length  $L$  is  $0.021 \leq \frac{r}{L} \leq 0.289$ . Table 2 presents statistic results for the three surfaces in Fig. 5, in which  $(\cdot)_0$  and  $(\cdot)_\infty$  are the minimal and maximal values respectively.

We also test our reconstruction algorithm on several point cloud models (Fig. 6), and compare our results with other reconstruction methods such as the ball-pivoting algorithm [14] and Crust algorithm [5]. As shown in Fig. 6, three different reconstruction results of the sphere-like model, the Monique model and the squirrel model are given, where in the first column is the point data, and the results in the second, third and fourth columns are generated by the ball-pivoting algorithm, Crust algorithm and our algorithm, respectively. These test examples show that, comparing to the other two reconstruction algorithms, our method generates comparative satisfactory results. All the reconstructions need only a few seconds of computing time.

The upsampling algorithm is performed and tested on the tri-torus surface (see Fig. 7). There are 6401 points in the initial point set (Fig. 7(b)), and after the upsampling procedure, the tri-torus point set (Fig. 7(d)) has 7547 points.

We also test our point sampling and reconstruction algorithms on surfaces (e.g. the dancer model in Fig. 8(a)) with features. It is worth pointing out that for surfaces without sharp features (see Fig. 8(a)), our algorithms could achieve a pleasing reconstruction result. See Fig. 8 for example, after sampling on the dancer model, the reconstruction preserves features of original surface (Fig. 8(c)) well.

The hole-filling algorithm comprises two steps: initial hole filling and refinement by solving a Poisson equation. In Fig. 9, (a) is the original retinal surface, (b) is the initial hole filling result, and (d) is the final result after the refinement by solving a Poisson equation. Note that our hole-filling algorithm is performed on point data, and the triangular meshes are the reconstruction results.

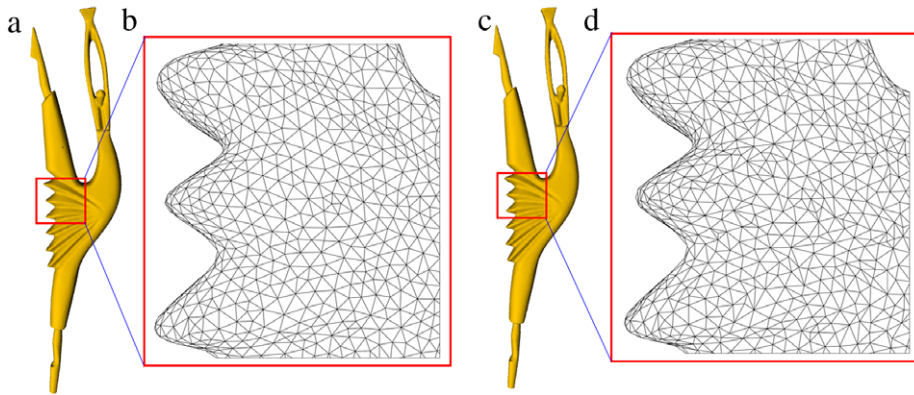


Fig. 8. (a) Original dancer model. (b) The local image of (a). (c) Reconstruction surface from sampling points of (a). (d) The local image of (c).

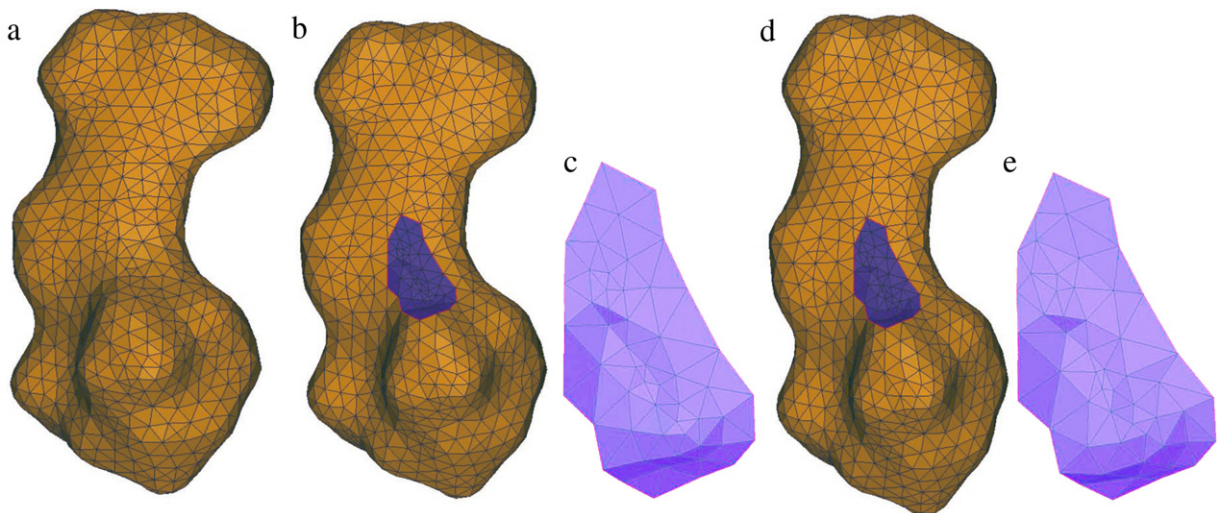


Fig. 9. (a) Original retinal surface. (b) Initial hole filling. (c) Hole patch in (b). (d) Final result. (e) Hole patch in (d).

## 5. Conclusions

In this paper, we propose a surface sampling criterion based on the injectivity radius, convexity radius and maximal principal curvature. We then establish the theoretical bounds of iDt mesh quality according to this sampling criterion. We also present an approximate iDt reconstruction algorithm for point data, and an upsampling procedure is proposed to convert point data into one satisfying our sampling criterion. Finally, a details-preserving hole-filling algorithm is used to complete point data with holes, and the repaired point data also satisfies the sampling criterion. In summary, the proposed sampling criterion can be used to guide many applications, including mesh reconstruction, point data upsampling and hole filling. Examples are presented to show the effectiveness of our methods.

## Acknowledgments

The authors would like to thank the reviewers for their constructive comments that helped to improve this paper. This work was partially supported by the Natural Science Foundation of China (61322206, 61373003), the National Basic Research Program of China (2011CB302202) and the National High Technology Research and Development Program of China (2012AA011801). The work of Y.J. Liu was supported in part by Beijing Higher Institution Engineering Research Center of Visual Media Intelligent Processing and Security, and Tsinghua University Initiative Scientific Research Program (20131089252).

## References

- [1] G. Leibon, D. Letscher, Delaunay triangulations and Voronoi diagrams for Riemannian manifolds, in: Proceedings of the Sixteenth Annual Symposium on Computational Geometry, 2000, pp. 341–349.
- [2] J. Dai, W. Luo, M. Jin, W. Zeng, Y. He, S.T. Yau, X. Gu, Geometric accuracy analysis for discrete surface approximation, *Comput. Aided Geom. Design* 24 (2007) 323–338.
- [3] N. Amenta, M. Bern, M. Kamvysellis, A new Voronoi-based surface reconstruction algorithm, in: SIGGRAPH '98: Proceedings of the 25th Annual Conference on Computer Graphics and Interactive Techniques, 1998, pp. 415–421.
- [4] R. Dyer, H. Zhang, T. Moller, Surface sampling and the intrinsic Voronoi diagram, in: Proceedings of the Symposium on Geometry Processing, 2008, pp. 1393–1402.
- [5] N. Amenta, S. Choi, One-pass Delaunay filtering for homeomorphic 3D surface reconstruction. UT report number TR99-08, 1999.
- [6] Y.J. Liu, Z.Q. Chen, K. Tang, Construction of iso-contours, bisectors and Voronoi diagrams on triangulated surfaces, *IEEE Trans. Pattern Anal. Mach. Intell.* 33 (8) (2011) 1089–1098.
- [7] Y.J. Liu, C.X. Xu, Y. He, D.S. Kim, The duality of geodesic Voronoi/Delaunay diagrams for an intrinsic discrete Laplace–Beltrami operator on simplicial surfaces, in: The 26th Canadian Conference on Computational Geometry, CCCG 2014, in press.
- [8] L.P. Chew, Guaranteed-quality mesh generation for curved surfaces, in: Proc. 9th Ann. Symp. Comput. Geom., 1993, pp. 274–280.
- [9] H. Edelsbrunner, N.R. Shah, Triangulating topological spaces, in: Proceedings of the Tenth Annual Symposium on Computational Geometry, 1994, pp. 285–292.
- [10] A.D. Aleksandrov, V.A. Zalgaller, *Intrinsic Geometry of Surfaces*, AMS Publisher, 1967.
- [11] Y.J. Liu, Exact geodesic metric in 2-manifold triangle meshes using edge-based data structures, *Comput.-Aided Des.* 45 (3) (2013) 695–704.
- [12] Y.J. Liu, K. Tang, The complexity of geodesic Voronoi diagrams on triangulated 2-manifold surfaces, *Inform. Process. Lett.* 113 (4) (2013) 132–136.
- [13] R. Kunze, F. Wolter, T. Rausch, Geodesic Voronoi diagrams on parametric surfaces, in: Proc. of Computer Graphics International, 1997, pp. 230–237.
- [14] F. Bernardini, J. Mittleman, H. Rushmeier, C. Silva, G. Taubin, The ball-pivoting algorithm for surface reconstruction, *IEEE Trans. Vis. Comput. Graphics* 5 (1999) 349–359.
- [15] H. Edelsbrunner, E.P. Mucke, Three-dimensional alpha shapes, *ACM Trans. Graph.* 13 (1) (1994) 43–72.
- [16] N. Amenta, M. Bern, Surface reconstruction by Voronoi filtering, *Discrete Comput. Geom.* 22 (1999) 481–504.
- [17] C.M. Gold, J. Snoeyink, A one-step crust and skeleton extraction algorithm, *Algorithmica* 30 (2) (2001) 144–163.
- [18] N. Amenta, S. Choi, T. Dey, N. Leekha, A simple algorithm for homeomorphic surface reconstruction, in: ACM Symposium on Computational Geometry, 2000, pp. 213–222.
- [19] T.K. Dey, S. Goswami, Provable surface reconstruction from noisy samples, *Comput. Geom. Theory Appl.* (2004).
- [20] T.K. Dey, J. Giesen, J. Hudson, Delaunay based shape reconstruction from large data, in: Proc. IEEE Symposium in Parallel and Large Data Visualization and Graphics, 2001, pp. 19–27.
- [21] Y.J. Liu, M.F. Yuen, Optimized triangle mesh reconstruction from unstructured points, *Vis. Comput.* 19 (1) (2003) 23–37.
- [22] Q. Du, D. Wang, Recent progress in robust and quality Delaunay mesh generation, *J. Comput. Appl. Math.* 195 (1–2) (2006) 8–23.
- [23] P.M. Knupp, Algebraic mesh quality metrics, *SIAM J. Sci. Comput.* 23 (2002) 193–218.
- [24] S.C. Park, M.K. Park, M.G. Kang, Superresolution image reconstruction: a technical overview, *IEEE Signal Process. Mag.* 21 (36) (2003).
- [25] I. Chavel, *Riemannian Geometry: A Modern Introduction*, second ed., Cambridge, 2006.
- [26] M.P. Do Carmo, *Riemannian Geometry*, Birkhauser, 1992.
- [27] W. Klingenberg, *Riemann Geometry*, de Gruyter, Berlin, 1982.
- [28] L. Aloul, Gertjan Kloosterman, Cornelis Traas, Ruud van Damme, Best data-dependent triangulations, *J. Comput. Appl. Math.* 119 (1) (2000) 1–12.
- [29] N. Dyn, D. Levin, S. Rippa, Boundary correction for piecewise linear interpolation defined over data-dependent triangulations, *J. Comput. Appl. Math.* 39 (2) (1992) 179–192.
- [30] Y.J. Liu, J.B. Zhang, J.C. Hou, J.C. Ren, W.Q. Tang, Cylinder detection in large-scale point cloud of pipeline plant, *IEEE Trans. Vis. Comput. Graphics* 19 (10) (2013) 1700–1707.
- [31] S. Park, X.H. Guo, H. Shin, H. Qin, Shape and appearance repair for incomplete point surfaces, in: The Tenth IEEE International Conference on Computer Vision, 2005, pp. 1260–1267.
- [32] C.S. Chong, Automatic mesh repair and optimisation for quality mesh generation. NUS, mechanical engineering (Ph.D. thesis), 2008.
- [33] M. Belkin, J. Sun, Y.S. Wang, Constructing Laplacian operator from point clouds in  $R^d$ , in: Proc. 20th, Ann. Symp. Discrete Algorithm, 2009, pp. 1031–1040.